Millimeter-Wave Angle Estimation of Multiple Targets Using Space-Time Modulation and Interferometric Antenna Arrays

Stavros Vakalis[®], Graduate Student Member, IEEE, and Jeffrey A. Nanzer[®], Senior Member, IEEE

Abstract—A new method of angle estimation of multiple targets using a distributed interferometric antenna array and wideband space—time modulation generating a dynamic array pattern is presented in this work. Interferometric array measurements of angle of arrival are generally ambiguous in the presence of two or more targets. We propose a new method of mitigating ambiguities in interferometric measurements by multiplying the angle pseudo-spectra from multiple antenna baselines, resulting in detections at only the angles of the targets. Using a single linear frequency-modulated transmitter and a receive interferometric array with N elements, we show a simple and computationally efficient technique to estimate the angle of up to $\mathcal{O}(N^2)$ targets. We describe the theory behind the technique, present detailed simulations, and provide an experimental verification using a three-element millimeter-wave measurement system.

Index Terms—Angle estimation, correlator arrays, dynamic arrays, interferometric antenna arrays, interferometry, radar, space-time modulation, target detection.

I. INTRODUCTION

R ADAR systems performing angle estimation have traditionally been used in applications that require all-weather capabilities for monitoring a spatial environment, such as air traffic control [1], [2], automotive radar [3], [4], intruder detection [5], and wireless sensor networks [6], [7]. Compared to the measurement of relative velocity and range, angle estimation is a more complicated measurement to implement with high accuracy, and traditionally has required some form of spatial scanning or digital receive array computational techniques such as eigenvalue decomposition. Mechanical scanning systems with rotating gimbals represent a simple and cost-effective solution for angle estimation, however these systems tend to be bulky, too slow for many applications, require additional power for mechanical gimbals, and are limited by the angular resolution of the antenna. A way to increase the analog beam-scanning speed is to use electronically scanning phased arrays [8]-[10], which can achieve improved gain,

Manuscript received February 26, 2021; revised May 27, 2021; accepted June 8, 2021. Date of publication July 12, 2021; date of current version November 4, 2021. This work was supported by the National Science Foundation under Grant 1751655. (Corresponding author: Jeffrey A. Nanzer.)

The authors are with the Department of Electrical and Computer Engineering, Michigan State University, East Lansing, MI 48824 USA (e-mail: vakaliss@msu.edu; nanzer@msu.edu).

Color versions of one or more figures in this article are available at https://doi.org/10.1109/TMTT.2021.3092359.

Digital Object Identifier 10.1109/TMTT.2021.3092359

spatial selectivity, and significantly faster scanning speeds than mechanically actuated systems. Nevertheless, phased antenna arrays require a large number of active components and a multielement filled aperture, which results in high cost [11]. The speed of electronic beam scanning can furthermore be restricting because all elements in a scanning phased array are capturing information associated with one angle at a time. Digital beamforming provides an alternative to analog beam scanning, and can simultaneously form beams corresponding to all angles in the field of view, however this approach necessitates the use of element-level digitization, which can lead to very high cost for typical filled array sizes [12].

Estimating target angle without beam scanning can significantly increase the capabilities of remote sensing systems. Subspace techniques such as MUSIC [13] and ESPRIT [14] have been extensively used for angle estimation without beam scanning, and can achieve resolution smaller than the diffraction limit of the aperture. However, these approaches leverage a priori information about the number of sources, which is not always available, and by using N antenna elements they cannot in general estimate the angle of more than N-1sources. Interferometric techniques such as very long baseline interferometry have been used in radio astronomy in order to reconstruct images of the stars and other stellar objects as a function of angle using far fewer elements than phased arrays [15], however such systems collect spatio-temporally incoherent thermal radiation to generate images using the Van Cittert-Zernike theorem [16], which necessitates very high sensitivity receivers. Multiple-input multiple-output (MIMO) radar using an M-element transmit array with diverse transmit waveforms and antenna spacings [17] can resolve the angle of a number of targets on the order of up to $\mathcal{O}(MN)$ [18]–[20]. This improvement comes with the additional hardware of a transmit array, which is not only costly but also power hungry, and increases the total system complexity. The concept of using multiplications between smaller element groups inside an antenna array to get narrower beams than typical linear array has been studied previously [21]. Effectively, this approach uses the concept of radiation pattern multiplication of phased subarrays, but typically it comes at the cost of increased sidelobe level [22], [23]. Co-prime and nested array processing can combine the information from two antenna arrays with M and N elements, respectively, in order

0018-9480 © 2021 IEEE. Personal use is permitted, but republication/redistribution requires IEEE permission. See https://www.ieee.org/publications/rights/index.html for more information.

to achieve target identifiability on the order of $\mathcal{O}(MN)$ in a completely passive setting [24]–[26]. This removes the need for expensive active hardware but can require computationally expensive signal processing and additional information such as higher order statistics.

We present a novel technique for estimating the angle of multiple targets using a single transmitter and an N-element interferometric receive array. Using a linear frequency-modulated (LFM) transmit waveform, the pair-wise cross correlation of the signals received by the array results in a dynamic radiation pattern that imparts a deterministic angular signature as a function of angle. By combining multiple baseline responses, the angle of up to $\mathcal{O}(N^2)$ targets can be accurately estimated. The technique uses interferometric processing that can achieve fast and accurate measurements with a simple hardware architecture. Unlike many direction-finding phase interferometry techniques, most of which are passive and only estimate the angles of emitting targets [27]–[30], our approach actively transmits a signal, thus it is possible to estimate the angle of any reflecting targets, not just emitting targets. However, because interferometric techniques can be ambiguous, we propose an approach to filter out the unwanted ambiguities by multiplying the responses from multiple baselines. Furthermore, unlike beam-scanning techniques that focus all the radiation at an angular direction at every instance, interferometric arrays capture information from the entire angular space simultaneously, which therefore significantly shortens the data acquisition time. By using only a single transmitter, our approach requires significantly less hardware than MIMO radar, and our signal-processing approach, based on vector multiplications and fast Fourier transforms, is fast and efficient. The benefits of our approach can be summarized as follows.

- 1) The technique can differentiate between the angle of $\mathcal{O}(N^2)$ targets with an N-element receive array and a single transmitter, compared to $\mathcal{O}(N)$ with conventional beamformers and subspace techniques, and $\mathcal{O}(MN)$ with MIMO radar with M transmitters.
- 2) The technique uses no electronic or mechanical beam scanning, which can limit observation time and can require additional electronic hardware [11].
- 3) The digital signal-processing algorithm is fast and simple and is based only on 1D element-by-element multiplications and Fourier transforms. It does not require eigenvalue decomposition, processing of two-dimensional covariance matrices, or matrix inversion like other approaches [13], [31], [32].

Previously we described the general operational concept and presented simulated and experimental results [33]. In the following, we describe in detail the theory behind interferometric angle estimation and the approach for mitigating unwanted ambiguous target responses. We present detailed simulations of angle estimation and assess the angle estimation root-mean-square error (RMSE) and probability of false alarm ($P_{\rm FA}$). Finally, we present a proof-of-concept demonstration using a three-element millimeter-wave experimental system.

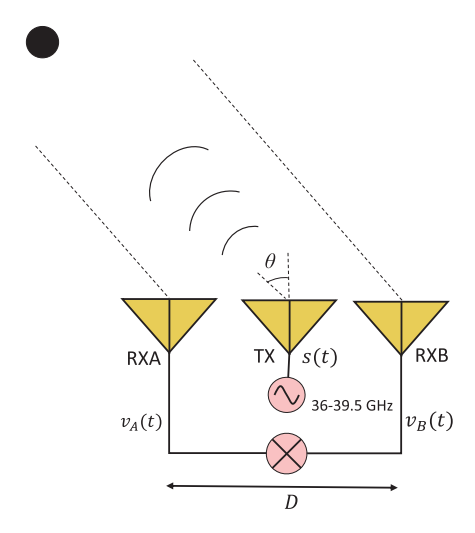


Fig. 1. Active interferometric array observing a target at angle θ . The transmitter generates an LFM waveform over the 36–39.5 GHz band, which is received by the two receiver antennas separated by the baseline D.

II. INTERFEROMETRIC ANGLE ESTIMATION USING DYNAMIC ARRAY PATTERNS

Simple and accurate angle estimation can be accomplished using a interferometric array and wideband spatial frequency modulation [34]. A single transmitter emitting an LFM signal and two receive antennas separated by a baseline D is shown in Fig. 1. The transmit signal is reflected from a target in the far-field at an angle θ and the two received signals are cross-correlated, which is realized by multiplication and low-pass filtering. The transmitted LFM signal s(t) can be written as

$$s(t) = \cos\left[2\pi\left(f_0t + \frac{\gamma}{2}t^2\right)\right] \tag{1}$$

where f_0 is the carrier frequency, and γ (Hz/s) is the chirp rate. The in-phase received signals on the two antennas separated by a baseline D after reflecting off of a point source residing at angle θ can be given by

$$v_A(t) = \cos\left[2\pi\left(f_0t + \frac{\gamma}{2}t^2\right)\right] + n_A(t) \tag{2}$$

$$v_A(t) = \cos\left\{2\pi\left[f_0(t - \tau_g) + \frac{\gamma}{2}(t - \tau_g)^2\right]\right\} + n_B(t)$$
 (3)

where $\tau_g = (D/c) \sin \theta$ represents the geometrical time delay of the wavefront from the target between the two antenna elements, c is the wavefront propagation speed, and $n_A(t)$, $n_B(t)$ are the noise components on receiver A and B. The in-phase part of the cross correlation of the two received signals can be written as

$$r^{I}(\tau_{g}) = \langle v_{A}(t)v_{B}(t)\rangle$$

$$= \left\langle \cos \left\{ 2\pi \left[f_{0}t + \frac{\gamma}{2}t^{2} \right] \right\} \cdot \left[\cos \left\{ 2\pi \left[f_{0}(t - \tau_{g}) + \frac{\gamma}{2}(t - \tau_{g})^{2} \right] \right\} \right\rangle$$

$$= \cos \left[2\pi \left(f_{0} + \gamma t - \frac{\gamma}{2}\tau_{g} \right) \tau_{g} \right]$$
(4)

where the angled brackets $\langle \cdot \rangle$ indicate time averaging, which can be accomplished with low-pass filtering. The noise terms do not show up in (4) because they are uncorrelated with each other and with the received signal and thus tend to zero with

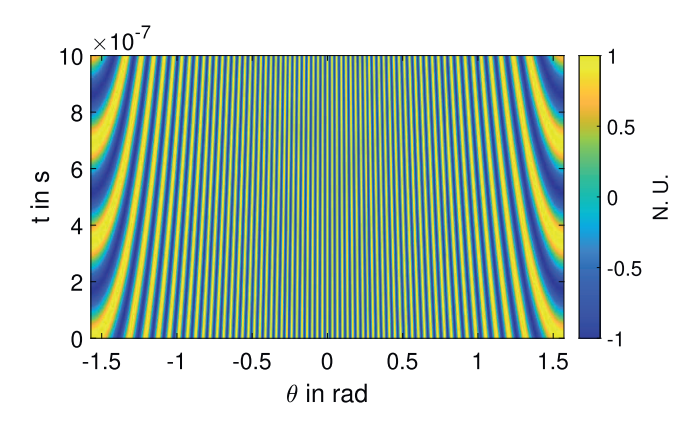


Fig. 2. Dynamic radiation pattern of a correlation interferometer with $D=0.25~\mathrm{m}$ and frequency ranging from 36 to 39.5 GHz. The real part of the electric field is plotted in normalized units (N.U.). As time increases more grating lobes appear in the spatial domain, introducing a space–time modulation that yields a unique signature as a function of angle.

sufficiently long integration time (or, equivalently, sufficiently low cutoff frequency in the low pass filter). Low-pass filtering also removes the higher frequency carrier components.

Combining the in-phase and quadrature outputs of the cross correlation produces the complex signal response

$$r(\tau) = e^{j2\pi \left(f_0 + \gamma t - \frac{\gamma}{2}\tau_g\right)\tau_g}.$$
 (5)

The instantaneous frequency f_i of the receiver circuit output can be found from the derivative of the phase through

$$f_i = \frac{1}{2\pi} \frac{d\phi}{dt} = \gamma \, \tau_g = \gamma \, \frac{D}{c} \sin \theta. \tag{6}$$

The target angle is then obtained through

$$\theta = \sin^{-1} \left(\frac{f_i c}{\gamma D} \right). \tag{7}$$

The instantaneous frequency is proportional to the chirp rate γ , the baseline D (in meters), and the sine of the angle θ at which the reflecting target resides. For angles $\theta \in$ $[(-\pi/2), (\pi/2)]$, each angular point has a unique frequency response as a function of time. Fig. 2 shows the resulting space-time dynamic array pattern as a function of time and one angular dimension. It can be seen that more grating lobes manifest as time increases. This is because the instantaneous frequency of the LFM signal increases linearly, and as a result the electrical baseline for two fixed antenna elements follows the same linear response. A two-element correlation interferometer with linearly increasing carrier frequency introduces a space-time modulation that manifests a unique sinusoidal response per angle. This leads to a simple and accurate angle estimation approach by simply estimating the frequency of the received signal, which uniquely matches a specific

The result in (7) assumes that the target is in the far-field region such that the reflections from the target obey the plane wave approximation, where the geometric time delay is given by

$$\tau_g = \frac{D}{c} \sin \theta. \tag{8}$$

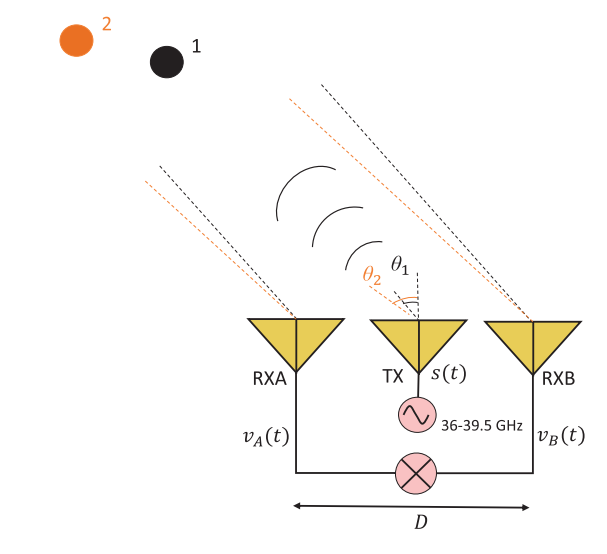


Fig. 3. Active distributed array observing two targets at angles θ_1 and θ_2 .

In the near-field, $\tau_g \approx (D/c) \sin \theta$ for angles close to broadside ($\theta = 0^{\circ}$) with minimal error [35]. For a moving target at angle θ the received signals can be written as

$$v_A(t) = \cos\left[2\pi \left(f_0 t + \frac{\gamma}{2} t^2 + f_{DA}\right)\right] + n_A(t)$$

$$v_B(t) = \cos\left\{2\pi \left[f_0 (t - \tau_g) + \frac{\gamma}{2} (t - \tau_g)^2 + f_{DB}\right]\right\} + n_B(t)$$
(10)

where $f_{\rm DA}=(2\ v_A/c)f_c$ and $f_{\rm DB}=(2\ v_B/c)f_c$ are the Doppler frequencies corresponding the radial velocity components v_A and v_B of the target observed from the received antennas A and B, respectively. The target angle will be successfully obtained if the two Doppler frequencies $f_{\rm DA}$ and f_{DB} are approximately equal. This is in general true in the far-field region; however, additional techniques may be needed such as varying the integration time (or pulse length) in order to adjust the frequency resolution and contain possible Doppler frequency offsets.

One challenge with the interferometric approach is that in general, it cannot unambiguously estimate the angle of more than one target. Consider the configuration of a two-element correlation interferometer receiver and a single transmitter observing the reflections from two targets 1 and 2 as shown in Fig. 3. Given the transmit LFM signal, the normalized signal responses in the two receive elements can be found as

$$v_{A}(t) = \cos\left\{2\pi \left[f_{0}(t - \tau_{A1}) + \frac{\gamma}{2}(t - \tau_{A1})^{2}\right]\right\} + \cos\left\{2\pi \left[f_{0}(t - \tau_{A2}) + \frac{\gamma}{2}(t - \tau_{A2})^{2}\right]\right\} + n_{A}(t)$$

$$v_{B}(t) = \cos\left\{2\pi \left[f_{0}(t - \tau_{B1}) + \frac{\gamma}{2}(t - \tau_{B1})^{2}\right]\right\} + \cos\left\{2\pi \left[f_{0}(t - \tau_{B2}) + \frac{\gamma}{2}(t - \tau_{B2})^{2}\right]\right\} + n_{B}(t)$$
(12)

where the terms τ_{Ai} , τ_{Bi} represent the total round trip time delays between the signal transmission and the reflection from the *i*th target arriving at the antenna elements A and B,

respectively. The output of the cross correlation of the two in-phase signals is then

$$r^{I} = \langle v_{A}(t)v_{B}(t) \rangle$$

$$= \left\langle \left(\cos \left\{ 2\pi \left[f_{0}(t - \tau_{A1}) + \frac{\gamma}{2}(t - \tau_{A1})^{2} \right] \right\} + \cos \left\{ 2\pi \left[f_{0}(t - \tau_{A2}) + \frac{\gamma}{2}(t - \tau_{A2})^{2} \right] \right\} \right)$$

$$\cdot \left(\cos \left\{ 2\pi \left[f_{0}(t - \tau_{B1}) + \frac{\gamma}{2}(t - \tau_{B1})^{2} \right] \right\} + \cos \left\{ 2\pi \left[f_{0}(t - \tau_{B2}) + \frac{\gamma}{2}(t - \tau_{B2})^{2} \right] \right\} \right). \quad (13)$$

Combining the in-phase and quadrature correlator outputs results in the complex signal response

$$r(\tau) = e^{j2\pi \left(f_0(\tau_{B1} - \tau_{A1}) + \gamma t(\tau_{B1} - \tau_{A1}) - \frac{\gamma}{2}(\tau_{B1}^2 - \tau_{A1}^2) \right)} + e^{j2\pi \left(f_0(\tau_{B2} - \tau_{A2}) + \gamma t(\tau_{B2} - \tau_{A2}) - \frac{\gamma}{2}(\tau_{B2}^2 - \tau_{A2}^2) \right)} + e^{j2\pi \left(f_0(\tau_{B2} - \tau_{A1}) + \gamma t(\tau_{B2} - \tau_{A1}) - \frac{\gamma}{2}(\tau_{B2}^2 - \tau_{A1}^2) \right)} + e^{j2\pi \left(f_0(\tau_{A2} - \tau_{B1}) + \gamma t(\tau_{A2} - \tau_{B1}) - \frac{\gamma}{2}(\tau_{A2}^2 - \tau_{B1}^2) \right)}.$$
 (14)

The instantaneous frequencies of the four terms in (14) can be found from the derivative of the phase to be $\gamma (\tau_{B1} - \tau_{A1})$, γ ($\tau_{B2} - \tau_{A2}$), γ ($\tau_{B2} - \tau_{A1}$), and γ ($\tau_{A2} - \tau_{B1}$) respectively. The first two terms $\gamma (\tau_{B1} - \tau_{A1})$ and $\gamma (\tau_{B2} - \tau_{A2})$ correspond to the geometric time-delay terms $\gamma(D/c)\sin\theta_1$ and $\gamma(D/c)\sin\theta_2$, and they represent the useful information that we need to capture in order to estimate the angle of the two targets. The last two terms $\gamma (\tau_{B2} - \tau_{A1})$ and $\gamma (\tau_{A2} - \tau_{B1})$ do not match the angle of any of the targets present in the scene, and they cannot be differentiated from the actual frequency responses that represent target angles. These terms come from the difference in round trip times of the signal reflected from target 2 to reach antenna element B and the response from target 1 to receive antenna element A, and vice versa. In general, when capturing the reflections from K targets, up to K^2 different frequency responses may manifest in the correlator output.

When a pair of receive antennas A and B are observing the reflections from K targets, the two complex voltages on receive antenna elements A and B can be written as

$$v_A(t) = \sum_{i=1}^{K} e^{j2\pi \left(f_0(t - \tau_{Ai}) + \frac{\gamma}{2}(t - \tau_{Ai})^2\right)}$$
 (15)

$$v_B(t) = \sum_{i}^{K} e^{j2\pi \left(f_0(t - \tau_{Bi}) + \frac{\gamma}{2}(t - \tau_{Bi})^2\right)}.$$
 (16)

And the correlator complex response can be written as

$$r(\tau) = \left\langle \sum_{i}^{K} e^{j2\pi \left(f_{0}(t - \tau_{Ai}) + \frac{\gamma}{2}(t - \tau_{Ai})^{2} \right)} \right.$$

$$\cdot \sum_{i}^{K} e^{j2\pi \left(f_{0}(t - \tau_{Bi}) + \frac{\gamma}{2}(t - \tau_{Bi})^{2} \right)} \right\rangle$$

$$= \sum_{i}^{K} e^{j2\pi \left(\gamma t (\tau_{Bi} - \tau_{Ai}) + \phi_{ii} \right)}$$

$$+ \sum_{i \neq i}^{K(K-1)} e^{j2\pi \left(\gamma t (\tau_{Bi} - \tau_{Aj}) + \phi_{ij} \right)}$$
(17)

where $\phi_{ii} = f_0(\tau_{Bi} - \tau_{Ai}) - (\gamma/2)(\tau_{Bi}^2 - \tau_{Ai}^2)$ and $\phi_{ij} = f_0(\tau_{Bi} - \tau_{Aj}) - (\gamma/2)(\tau_{Bi}^2 - \tau_{Aj}^2)$. Thus for K targets on different angles we will have K desired frequency responses $\sum_i^K e^{j2\pi(\gamma t(\tau_{Bi} - \tau_{Ai}) + \phi_{ii})}$ and up to K(K-1) undesired frequency responses $\sum_{i \neq j}^{K(K-1)} e^{j2\pi(\gamma t(\tau_{Bi} - \tau_{Aj}) + \phi_{ij})}$. It is theoretically possible for intermodulation responses to manifest at the same frequency or within the resolution limit, producing less than K(K-1) responses. The next section describes a multibaseline approach to mitigate these false angle responses.

III. DISAMBIGUATION USING MULTIPLE INTERFEROMETRIC BASELINES

An instantaneous frequency response of a target at angle θ , given by (6), can have only values such that $f_i \in [-\gamma(D/c), \gamma(D/c)]$ for $-1 \le \sin \theta \le 1$. So, for two targets A and B and for a two element interferometer, if $(\tau_{B2} - \tau_{A1})$ and $(\tau_{A2} - \tau_{B1})$ are both larger than D/c, then they could simply be ignored as a potential target response because they do not correspond to a real angle. This approach will potentially filter out some unwanted information, especially for small baselines D. However, false target angles will generally not always manifest at angles outside of the real range, especially for a large number of targets K where the number of unwanted cross-product frequency responses can be up to K(K-1).

Our solution starts with the use of an interferometric array instead of a single correlation interferometer. An antenna array with N elements that uses interferometric processing can have up to (1/2)N(N-1) unique baselines, because the pairwise processing between the N elements yields up to $\binom{N}{2}$ unique pairs. Actual target responses will manifest at the same locations of the angle pseudo-spectrum in all different baselines of the array, however the unwanted cross-product terms will not manifest on all antenna baselines at the same locations of the angular spectrum. Thus, the desired true angle information will appear consistently in all different baselines, however this is not the case for the unwanted cross-products terms. We thus multiply the responses of the multiple baselines, resulting in large signal power for the true target signals that are consistent in angle across all baselines, and reducing the signal power of the false angle targets, at which angles most baselines have a low signal amplitude.

The algorithm is described visually in Fig. 4. The receive antenna elements capture the reflections of the transmitted signals from the targets in front of the array. The responses of each element are captured, multiplied pair-wise, and low-pass filtered to produce the (1/2)N(N-1) correlation interferometer output. The output of each correlation interferometer is then Fourier transformed and converted to the angle spectrum using (7). By multiplying the angle spectra, only the common responses are retained from the (1/2)N(N-1) spectra, because for most baselines the false angle responses are of low amplitude. The process thus works like a filter in the angular pseudo-spectrum. It should be noted that our processing is different than traditional multiplicative arrays [21] where multiplication takes place between subsets of the antenna elements and the synthesized beam is scanned in space. In our technique

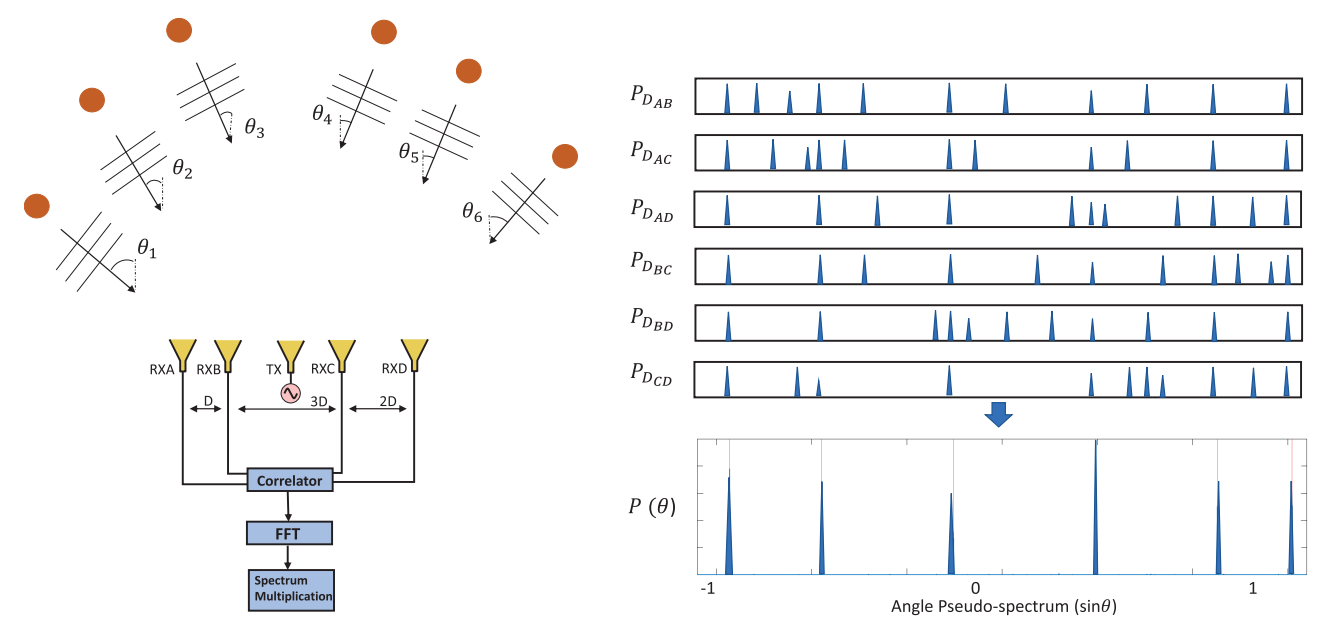


Fig. 4. (Left) N = 4-element receive array with a single transmitter observing the reflections from (1/2)N(N-1) = 6 targets. The received signals are cross correlated pairwise and the cross-correlation outputs are Fourier transformed to convert them to angle pseudo-spectra, which are multiplied to keep only the useful angle information. (Right) Qualitative visualization of the six individual baselines that contain both the useful and unwanted frequency information. The bottom plot shows the multiplicative correlation response, which retains only the signal responses at the true target angles.

we use no beam-scanning and our subsets are not multielement sets, but rather two-element interferometers.

For (1/2)N(N-1) baselines the multiplicative output can be written as a Hadamard product between the angular pseudo-spectra of the antenna baselines $P_{D_{AB}}$, $P_{D_{AC}}$, $P_{D_{AD}}$ until all pairs have been utilized

$$P(\theta) = P_{D_{AB}}(\theta) \odot P_{D_{AC}}(\theta) \odot P_{D_{AB}}(\theta) \odot \cdots$$
 (18)

Given that we resolve target angles through frequency estimates, two targets separated in angle by $\Delta\theta$ will have differences in frequency given by

$$\Delta f = \gamma \frac{D_{\text{max}}}{c} [\sin(\theta + \Delta \theta) - \sin \theta]$$
 (19)

where $D_{\rm max}$ is the maximum baseline in the array. If $\Delta\theta$ is small, $\sin(\theta + \Delta\theta)$) $-\sin\theta \approx \Delta\theta\cos\theta$ and $\Delta f = (1/T)$, where T is the period of the LFM signal, and thus we can write the resolution as

$$\Delta\theta = \frac{c}{\gamma T D_{\text{max}} \cos \theta}.$$
 (20)

Near broadside to the array, $\cos \theta \approx 1$; substituting γT with the signal bandwidth B we can estimate the angular resolution of this technique as

$$\Delta\theta = B_f^{-1} \frac{\lambda}{D_{\text{max}}} \tag{21}$$

where $B_f = B/f_c$ is the signal fractional bandwidth compared to the center carrier frequency f_c . The calculated resolution for practical applications is larger than the typical diffraction limited resolution, which can be approximated as the 3-dB beamwidth of an aperture $\theta_{3dB} = 0.886(\lambda/D_{\rm max})$ [36], [37]. However, our technique uses no beam scanning and claims superior target identifiability compared to other array techniques. In the next section we demonstrate through simulation

the ability to accurately estimate multiple target angles for arrays with N elements when observing number of targets even larger than (1/2)N(N-1) under various signal-to-noise ratio (SNR) scenarios.

IV. SIMULATED ANGLE RECONSTRUCTIONS OF $\mathcal{O}(N^2)$ Targets

Simulations were run in MATLAB for an antenna array with N = 4 elements $\{A, B, C, D\}$ with spacings $\{2D, 3D,$ 5D}, where D = 1 m. An SNR of 5 dB was implemented. Because the angle-dependent responses manifest as a function of the chirp rate, and not the carrier frequency, the simulations were conducted at baseband. The bandwidth of the LFM chirp was 4 GHz, and the pulse repetition interval was 1 μ s, resulting in a chirp rate $K = 4 \cdot 10^{15}$ Hz/s. The response from (1/2)N(N-1) = 6 targets at angles -63° , -36° , -9° , 18°, 45°, and 72° with identical radar cross section (RCS) can be seen in Fig. 5. The individual correlator responses each show signals at the target angles (represented by red lines) and a number of false responses at other angles. The resulting multiplicative correlator response retains only the true target angle responses. We note that while the reflectivities of each target were identical, the resultant amplitudes of the signals in the multiplicative correlator response are not; this is because of the interference generated by false target responses in some of the individual correlator responses. Nonetheless, the resultant responses of the true target angles show significantly higher signal strength than the noise floor, even at 5 dB SNR, leading to robust detection. Furthermore, we note that typical array-based angle estimation techniques also do not reconstruct target amplitudes [13], [14].

To investigate how our technique performs with targets of varying RCS, we simulated the same array with spacings $\{2D, 3D, 5D\}$, where D = 1 m, and 4 GHz of bandwidth.

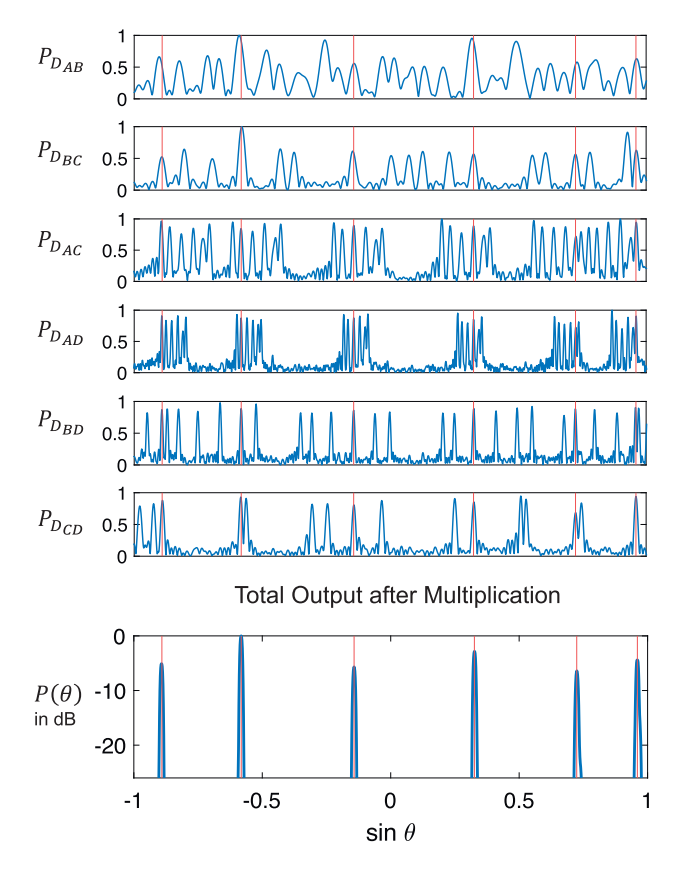


Fig. 5. Simulated results for a 4-element receive interferometric array with elements $\{A, B, C, D\}$ in spacings $\{2D, 3D, 5D\}$ observing the responses from (1/2)N(N-1)=6 targets with identical RCS, indicated with red lines, with SNR = 5 dB. Although each baseline has unwanted cross-product terms, in the bottom it can be seen that only the responses from the six targets remain.

The SNR was 5 dB. The six targets were located at the same angles, however their RCS varied from 5 to 10 dB, increasing by 1 dB for the targets at angles from -90° to 90° . The results can be seen in Fig. 6. Our technique is able to reconstruct the residing angle of targets of varying RCS, however it does not inherently estimate the target amplitude. Small artifacts appear next to the two targets close to 90° ; such responses near strong targets may become comparable to the amplitude of the weakest targets in some cases.

Monte Carlo simulations were run for the same 4-element array observing the angle of six targets of the same RCS for 500 iterations and calculating the RMSE for different SNR values. The results are shown in Fig. 7, which show that the RMSE is constant for SNR values above 10 dB and is less than 0.04° for 0 dB SNR. Although there is no coherent processing such as matched filtering, the cross correlation applies some denoising to uncorrelated noise, which makes angle estimation possible even for SNR less than 0 dB, with RMSE less than 0.055° for -5 dB SNR. For SNR values smaller than -5 dB the RMSE becomes more significant.

With a large number of false target angles manifesting with increasing baselines and increasing number of targets, it is relevant to study this effect on the multiplicative correlator output in order to estimate when the ambiguity mitigation would start to fail. The probability of false alarm (P_{FA})

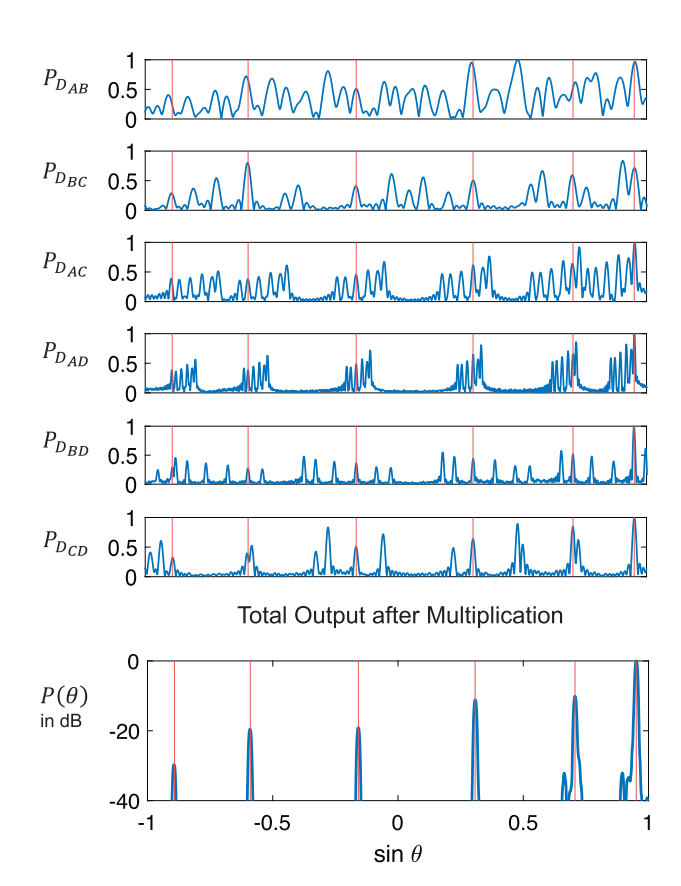


Fig. 6. Simulated results for a 4-element receive interferometric array with elements $\{A, B, C, D\}$ in spacings $\{2D, 3D, 5D\}$ observing the responses from (1/2)N(N-1)=6 targets with RCS values of 5,6,7,8,9, and 10 dB from left to right. The target angles are indicated with red lines, with SNR = 5 dB.

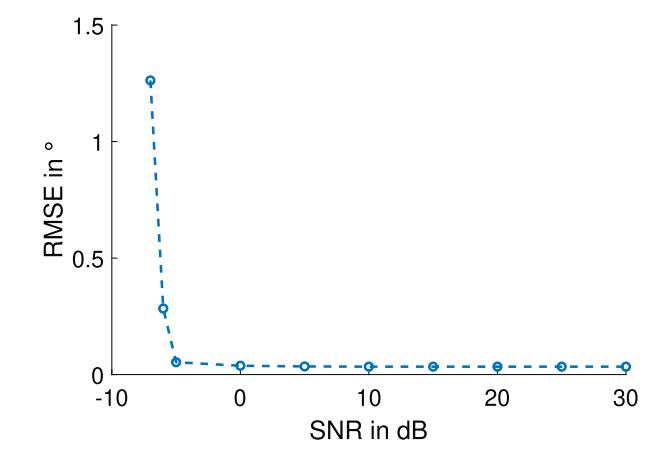


Fig. 7. RMSE plot for a 4-element array observing the responses from (1/2)N(N-1) = 6 targets. Because of the correlation process, this technique works well even at negative SNR values.

was thus evaluated for a 5-element receive array observing the reflection from K=8 to K=16 targets under various SNR scenarios. The array had spacings {2D, 3D, 5D, 7D} and D=5 m. The K targets were uniformly placed in the $[-90^{\circ}, 90^{\circ}]$ space and a random offset was applied at each Monte Carlo loop. The results of the simulation can be seen in Fig. 8. It can be seen that for positive SNR values the P_{FA} becomes negligible for number of targets up to K=14, which is larger than the number of baselines

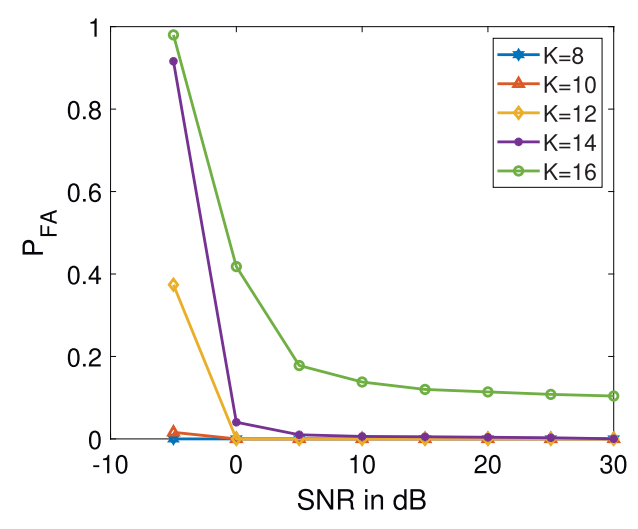


Fig. 8. Probability of false alarm (P_{FA}) for a 5-element array observing the reflections from K targets. The technique shows promising results even for $K \ge (1/2)N(N-1)$.

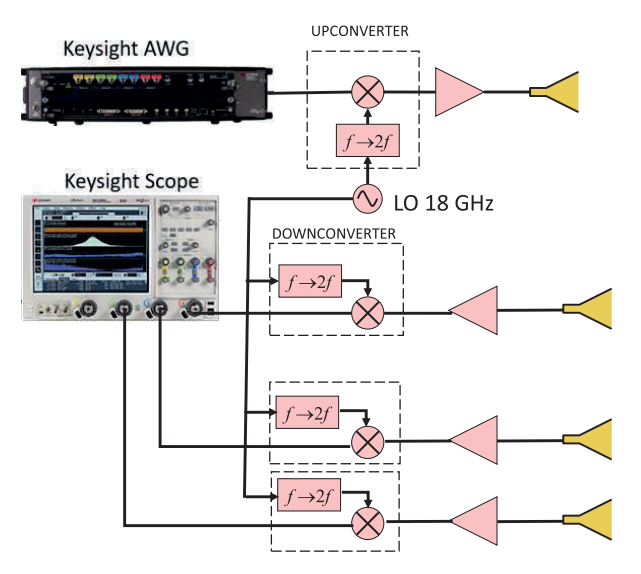


Fig. 9. Experimental 36–39.5-GHz configuration with one transmitter and three receivers. The transmit signal was generated at baseband using a Keysight M8190 AWG and the received signals were captured using a Keysight MSOX92004A mixed-signal oscilloscope.

(1/2)N(N-1) = 10. The ability to accurately estimate the angles of more targets than baselines in the array is significant, if not intuitive. However, we note that in this approach we are not limited by a system with (1/2)N(N-1) equations, thus it is not unreasonable to be able to solve for more than (1/2)N(N-1) unknowns. Essentially, the approach simply filters out unwanted responses, similar to a microwave filter removing spurious frequency responses, but in a dynamic way.

V. MILLIMETER-WAVE EXPERIMENTAL MEASUREMENTS

To verify our approach for angle estimation we built an experimental configuration, a schematic of which can be seen in Fig. 9. We used 15 dBi 3D printed horn antennas that were fabricated at Michigan State University [38]. The transmitted LFM signal was generated at baseband with a Keysight M8190 Arbitrary Waveform Generator (AWG). The signal had 3.5 GHz of bandwidth and a pulse duration of $100 \ \mu s$, which

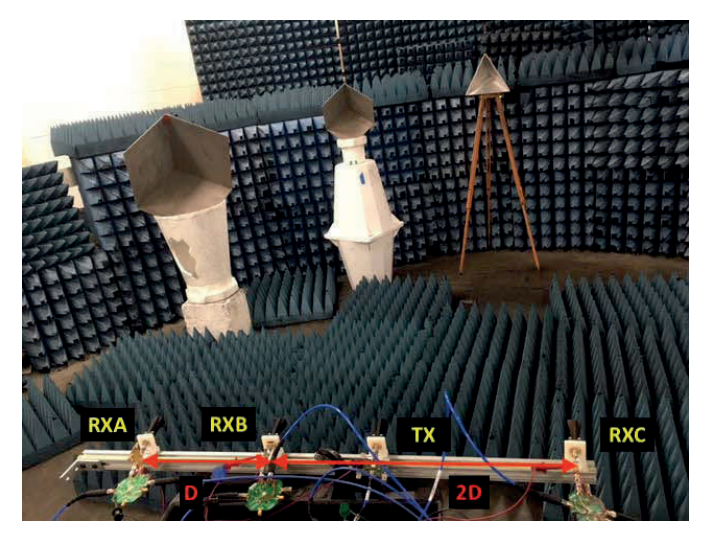


Fig. 10. Experimental measurements took place in a semianechoic environment with three corner reflectors at angles 0° , 12.5° , and 26° .

translated to a chirp rate of 3.5×10^{13} Hz/s. The upconversion to 36-39.5 GHz took place with an Analog Devices (ADI) HMC6787ALC5A upconverter and an ADI HMC7229 24 dB power amplifier was used for additional amplification at the carrier frequency. On the receive side, the signals were amplified by 23 dB gain ADI HMC1040LP3CE low-noise amplifiers at the output of the antennas and then downconverted using ADI HMC6789BLC5A downconverters. Both up- and down-converters included a frequency doubler; an 18-GHz local oscillator (LO) was used on both. The received signals were captured using a Keysight MSOX92004A mixed-signal oscilloscope and were processed offline in MATLAB.

Experimental measurements took place inside a 7.6-m semianechoic antenna range as shown in Fig. 10. Three corner reflectors were located at 0°, 12.5°, and 26° relative to the array broadside with RCS of 21, 33, and 41 dBsm, respectively. The receive antenna array consisted of three antenna elements spaced at baselines $\{D,2D\}$ with D =0.25 m and the transmit antenna was placed in the center of the array. The antennas were located on a linear grid with mm-level accuracy. Small antenna misplacements that are a fraction of wavelength can be tolerated, however antenna misplacements that cause frequency offsets comparable with the angular resolution can cause the individual spectra to misalign, degrading performance. The maximum separation of the array was 3D = 0.75 m and the angular resolution of the array can be calculated with (21) to be 6.55°. Although the measurement was taking place in the near-field of the receive array, the targets are sufficiently near broadside such that (8) approximately holds as discussed in Section II.

The frequency responses of the three correlation interferometers with baselines D, 2D, and 3D can be seen in Fig. 11, where the red dotted lines show the frequencies of the target responses. The frequency resolution is the inverse of the integration time and in our case was 10 kHz; an increased Fourier transform length was used to smooth the angular spectra. The smaller baseline with length *D* produces a coarse response and therefore cannot differentiate the three targets responses. The response from baseline with length 2D also

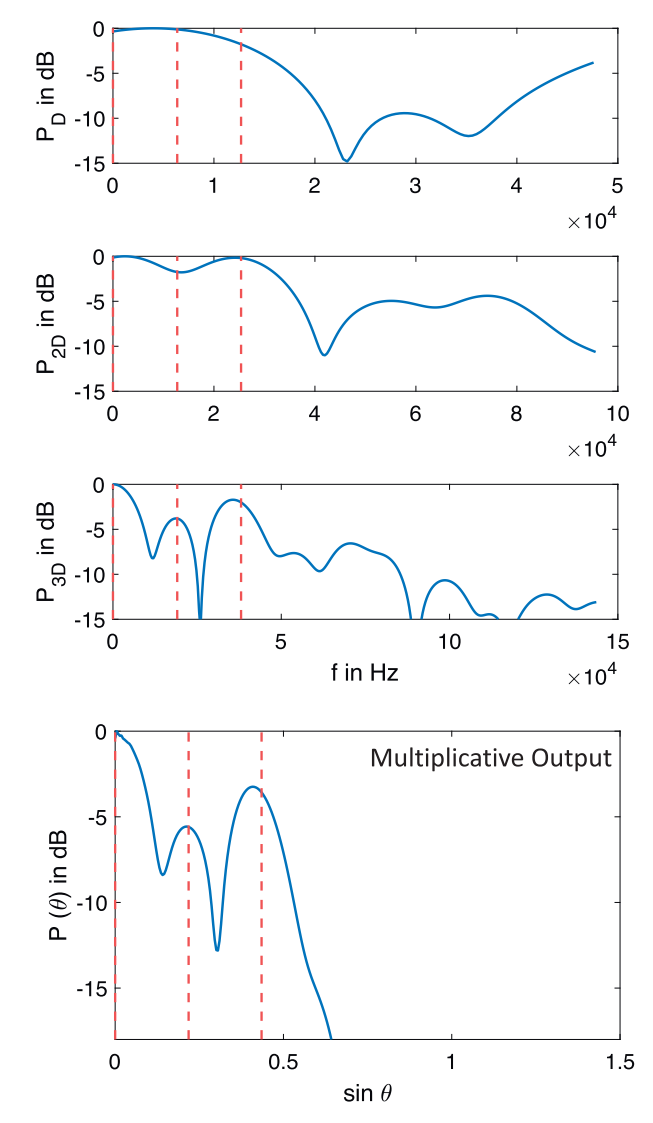


Fig. 11. (Top) Experimental frequency responses from three interferometers with baselines D, 2D, and 3D observing three targets at angles 0° , 12.5° , and 26° in dB. The vertical dotted red lines represent the frequency responses of the targets. (Bottom) Total system output after multiplying the three individual baseline responses. The unwanted cross-product information has been mitigated significantly and was pushed below -18 dB.

fails to generate sufficient responses to differentiate between all targets but provides a peak for the third target at 26°. The baseline with length 3D is able to differentiate between the three targets, however there are additional peaks, which do not correspond to targets present in the scene. The smaller peaks on the right side of the spectra for the baselines 2D and 3D do not appear in all three of the spectra and therefore do not represent information associated with the residing angle of a target present in the scene. In Fig. 11 (bottom) the multiplicative correlation response is shown, where the true target angles have been retained, and the additional false target responses have been pushed below -18 dB. The unwanted cross-product information has been mitigated significantly. Although $0 \le \sin \theta \le 1$, we have not cropped the horizontal axis to show that some filtering takes place from the responses that do not correspond to real angles. No denoising has been applied to the data, and this technique is able to run in

real time, as the signal processing is based on 1D vector multiplications and Fourier transforms.

VI. CONCLUSION

A novel active technique for angle estimation of multiple targets using an LFM transmit waveform and an interferometric array receiver with a dynamic array radiation pattern has been demonstrated. In contrast to other active angle estimation approaches, no beam-scanning is necessary in this technique. We introduced a method of filtering ambiguous responses by combining the common information from multiple baselines and the simulated and experimental results show good agreement. With our technique an array with N receivers can accurately estimate the angle of more than (1/2)N(N-1) targets. By demonstrating a simple and computationally efficient method of estimating the angles of multiple targets, this work may have impacts on applications such as sensing in wireless networks, air-traffic monitoring, personnel monitoring, home health, and sensing for ground and aerial vehicles. Although in this work we are concerned with angle estimation as the result of pairwise correlations in a sparse active array, future work will combine range estimates from individual receive antenna responses with the pairwise angle estimates in order to achieve two-dimensional mappings and target localization.

REFERENCES

- M. I. Skolnik, Introduction to Radar Systems. New York, NY, USA: McGraw-Hill, 2001.
- [2] C. R. Rao, L. Zhang, and L. C. Zhao, "Multiple target angle tracking using sensor array outputs," *IEEE Trans. Aerosp. Electron. Syst.*, vol. 29, no. 1, pp. 268–271, Mar. 1993.
- [3] J. Hasch, E. Topak, R. Schnabel, T. Zwick, R. Weigel, and C. Waldschmidt, "Millimeter-wave technology for automotive radar sensors in the 77 GHz frequency band," *IEEE Trans. Microw. Theory Techn.*, vol. 60, no. 3, pp. 845–860, Mar. 2012.
- [4] M. Steinhauer, H.-O. Ruoss, H. Irion, and W. Menzel, "Millimeter-waveradar sensor based on a transceiver array for automotive applications," *IEEE Trans. Microw. Theory Techn.*, vol. 56, no. 2, pp. 261–269, Feb. 2008.
- [5] D. Accardo, G. Fasano, L. Forlenza, A. Moccia, and A. Rispoli, "Flight test of a radar-based tracking system for UAS sense and avoid," *IEEE Trans. Aerosp. Electron. Syst.*, vol. 49, no. 2, pp. 1139–1160, Apr. 2013.
- [6] J.-F. Gu and P. Wei, "Joint SVD of two cross-correlation matrices to achieve automatic pairing in 2-D angle estimation problems," *IEEE Antennas Wireless Propag. Lett.*, vol. 6, pp. 553–556, 2007.
- [7] Y. Wu and H. C. So, "Simple and accurate two-dimensional angle estimation for a single source with uniform circular array," *IEEE Antennas Wireless Propag. Lett.*, vol. 7, pp. 78–80, 2008.
- [8] A. Clemente, L. Dussopt, R. Sauleau, P. Potier, and P. Pouliguen, "Wideband 400-element electronically reconfigurable transmitarray in X band," *IEEE Trans. Antennas Propag.*, vol. 61, no. 10, pp. 5017–5027, Oct. 2013.
- [9] B. Ku et al., "A 77–81-GHz 16-element phased-array receiver with ±50° beam scanning for advanced automotive radars," *IEEE Trans. Microw. Theory Techn.*, vol. 62, no. 11, pp. 2823–2832, Nov. 2014.
- [10] R. C. Hansen, *Phased Array Antennas*. Hoboken, NJ, USA: Wiley, 2009.
- [11] B. Avser, J. Pierro, and G. M. Rebeiz, "Random feeding networks for reducing the number of phase shifters in limited-scan arrays," *IEEE Trans. Antennas Propag.*, vol. 64, no. 11, pp. 4648–4658, Nov. 2016.
- [12] S. H. Talisa, K. W. O'Haver, T. M. Comberiate, M. D. Sharp, and O. F. Somerlock, "Benefits of digital phased array radars," *Proc. IEEE*, vol. 104, no. 3, pp. 530–543, Mar. 2016.
- [13] R. Schmidt, "Multiple emitter location and signal parameter estimation," *IEEE Trans. Antennas Propag.*, vol. AP-34, no. 3, pp. 276–280, Mar. 1986.
- [14] R. Roy and T. Kailath, "ESPRIT-estimation of signal parameters Via rotational invariance techniques," *IEEE Trans. Acoust., Speech, Signal Process.*, vol. 37, no. 7, pp. 984–995, Jul. 1989.

- [15] A. R. Thompson, J. M. Moran, and G. W. Swenson, *Interferometry and Synthesis in Radio Astronomy*. Hoboken, NJ, USA: Wiley, 2001.
- [16] M. Born and E. Wolf, *Principles of Optics*. Cambridge, U.K.: Cambridge Univ. Press, 1999.
- [17] J. Li and P. Stoica, "MIMO radar with colocated antennas," *IEEE Signal Process. Mag.*, vol. 24, no. 5, pp. 106–114, Sep. 2007.
- [18] J. Li, P. Stoica, L. Xu, and W. Roberts, "On parameter identifiability of MIMO radar," *IEEE Signal Process. Lett.*, vol. 14, no. 12, pp. 968–971, Dec. 2007.
- [19] R. Feger, C. Wagner, S. Schuster, S. Scheiblhofer, H. Jager, and A. Stelzer, "A 77-GHz FMCW MIMO radar based on an SiGe singlechip transceiver," *IEEE Trans. Microw. Theory Techn.*, vol. 57, no. 5, pp. 1020–1035, May 2009.
- [20] D. Bleh et al., "W-band time-domain multiplexing FMCW MIMO radar for far-field 3-D imaging," *IEEE Trans. Microw. Theory Techn.*, vol. 65, no. 9, pp. 3474–3484, Sep. 2017.
- [21] V. G. Welsby and D. G. Tucker, "Multiplicative receiving arrays," *J. Brit. Inst. Radio Eng.*, vol. 19, no. 6, pp. 369–382, Jun. 1959.
- [22] D. E. N. Davies and C. R. Ward, "Low sidelobe patterns from thinned arrays using multiplicative processing," *IEE Proc. F Commun., Radar Signal Process.*, vol. 127, no. 1, p. 9, 1980.
- [23] R. H. MacPhie and T. H. Yoon, "Grating lobe suppression with a thinned multiplicative receiving array," in *Proc. Asia–Pacific Microw. Conf.*, Dec. 2005, p. 4.
- [24] P. Pal and P. P. Vaidyanathan, "Nested arrays: A novel approach to array processing with enhanced degrees of freedom," *IEEE Trans. Signal Process.*, vol. 58, no. 8, pp. 4167–4181, Aug. 2010.
- [25] P. P. Vaidyanathan and P. Pal, "Sparse sensing with co-prime samplers and arrays," *IEEE Trans. Signal Process.*, vol. 59, no. 2, pp. 573–586, Feb. 2011.
- [26] K. Han, P. Yang, and A. Nehorai, "Calibrating nested sensor arrays with model errors," *IEEE Trans. Antennas Propag.*, vol. 63, no. 11, pp. 4739–4748, Nov. 2015.
- [27] J. Moghaddasi, T. Djerafi, and K. Wu, "Multiport interferometer-enabled 2-D angle of arrival (AOA) estimation system," *IEEE Trans. Microw. Theory Techn.*, vol. 65, no. 5, pp. 1767–1779, May 2017.
- [28] J.-H. Lee, J.-H. Lee, and J.-M. Woo, "Method for obtaining three- and four-element array spacing for interferometer direction-finding system," *IEEE Antennas Wireless Propag. Lett.*, vol. 15, pp. 897–900, 2016.
- [29] P. Q. C. Ly, "Fast and unambiguous direction finding for digital radar intercept receivers," M.S. thesis, School Elect. Electron. Eng., Univ. Adelaide, Adelaide, SA, Australia, 2013.
- [30] W. Stevers, A. Schlegel, P. Chatterjee, J. Opperman, and J. A. Nanzer, "Direction-of-arrival estimation using a low-cost, portable, software-defined-radio-based phase interferometry system [education corner]," IEEE Antennas Propag. Mag., vol. 61, no. 4, pp. 78–84, Aug. 2019.
- [31] J. Li, P. Stoica, and Z. Wang, "On robust capon beamforming and diagonal loading," *IEEE Trans. Signal Process.*, vol. 51, no. 7, pp. 1702–1715, Jul. 2003.
- [32] S. Haykin, Radar Array Processing (Springer Series in Information Sciences), vol. 25. Berlin, Germany: Springer, 1993. [Online]. Available: https://link.springer.com/10.1007/978-3-642-77347-1
- [33] S. Vakalis and J. A. Nanzer, "A space-time modulated distributed antenna array for multiple target angle estimation," in *Proc. IEEE Int.* Symp. Antennas Propag. North Amer. Radio Sci. Meeting, Jul. 2020, pp. 1089–1090.
- [34] S. Vakalis, E. Klinefelter, and J. A. Nanzer, "Angle estimation using wideband frequency modulation and an active distributed array," *IEEE Microw. Wireless Compon. Lett.*, vol. 28, no. 11, pp. 1059–1061, Nov. 2018.
- [35] J. A. Nanzer and R. L. Rogers, "A Ka-band correlation radiometer for human presence detection from a moving platform," in *IEEE MTT-S Int. Microw. Symp. Dig.*, Jun. 2007, pp. 385–388.
- [36] C. A. Balanis, Antenna Theory. Hoboken, NJ, USA: Wiley, 2012.
- [37] R. J. Mailloux, Phased Array Antenna Handbook. Norwood, MA, USA: Artech House, 2005.
- [38] J. A. Byford, M. I. M. Ghazali, S. Karuppuswami, B. L. Wright, and P. Chahal, "Demonstration of RF and microwave passive circuits through 3-D printing and selective metalization," *IEEE Trans. Compon., Packag., Manuf. Technol.*, vol. 7, no. 3, pp. 463–471, Mar. 2017.



Stavros Vakalis (Graduate Student Member, IEEE) received the diploma degree in electrical and computer engineering from the National Technical University of Athens, Athens, Greece, in 2017, and the M.S. degree in electrical and computer engineering from Michigan State University, East Lansing, MI, USA, in 2020, where he is currently pursuing the Ph.D. degree in electrical engineering.

His current research interests include wireless microwave and millimeter-wave systems, millimeterwave imaging, antenna arrays, and radar and signal

processing.

Mr. Vakalis is a member of the IEEE Microwave Theory and Techniques Society and the IEEE Antennas and Propagation Society. He received the Gerondelis Foundation Graduate Scholarship in 2019, the IEEE Microwave Theory and Techniques Society (IEEE MTT-S) Graduate Fellowship Award in 2021, and an URSI Young Scientist Award in 2021. He was the recipient of the Second Place Awards of both the Student Paper Competition and the Student Design Competition at the 2020 IEEE International Symposium on Antennas and Propagation, and the 2020-21 Fitch H. Beach Award for outstanding research in the College of Engineering, Michigan State University (Honorable Mention). He is currently serving as a Reviewer for the IEEE Transactions on Microwave Theory and Techniques, the IEEE JOURNAL OF ELECTROMAGNETICS, RF AND MICROWAVES IN MEDICINE AND BIOLOGY, the IEEE TRANSACTIONS ON ANTENNAS AND PROPAGATION, and the IEEE GEOSCIENCE AND REMOTE SENSING LETTERS.



Jeffrey A. Nanzer (Senior Member, IEEE) received the B.S. degrees in electrical engineering and computer engineering from Michigan State University, East Lansing, MI, USA, in 2003, and the M.S. and Ph.D. degrees in electrical engineering from The University of Texas at Austin, Austin, TX, USA, in 2005 and 2008, respectively.

From 2008 to 2009, he was a Post-Doctoral Fellow with Applied Research Laboratories, University of Texas at Austin, where he was involved in designing electrically small HF antennas and communication

systems. From 2009 to 2016, he was with The Johns Hopkins University Applied Physics Laboratory, Laurel, MD, USA, where he created and led the Advanced Microwave and Millimeter-Wave Technology Section. In 2016, he joined the Department of Electrical and Computer Engineering, Michigan State University, where he is currently the Dennis P. Nyquist Assistant Professor. He has authored or coauthored more than 150 refereed journal and conference articles, authored Microwave and Millimeter-Wave Remote Sensing for Security Applications (Artech House, 2012), and coauthored the chapter Photonics-Enabled Millimeter-Wave Wireless Systems in wireless transceiver circuits (Taylor & Francis, 2015). His current research interests include distributed arrays, radar and remote sensing, antennas, electromagnetics, and microwave photonics.

Dr. Nanzer is a member of the IEEE Antennas and Propagation Society Education Committee and the USNC/URSI Commission B. He was a Founding Member and the First Treasurer of the IEEE APS/ MTT-S Central Texas Chapter. He served as the Vice Chair for the IEEE Antenna Standards Committee from 2013 to 2015 and a Chair of the Microwave Systems Technical Committee (MTT-16), the IEEE Microwave Theory and Techniques Society from 2016 to 2018. He was a recipient of the Outstanding Young Engineer Award from the IEEE Microwave Theory and Techniques Society in 2019, the DARPA Director's Fellowship in 2019, the National Science Foundation (NSF) CAREER Award in 2018, the DARPA Young Faculty Award in 2017, and the JHU/APL Outstanding Professional Book Award in 2012. He is currently an Associate Editor of the IEEE TRANSACTIONS ON ANTENNAS AND PROPAGATION.